Final Technical Report

Molecular Characterization of Bacterial Respiration on Minerals

1. Summary/Overview of progress

The overall aim of this project was to contribute to our fundamental understanding of proteins and biological processes under extreme environmental conditions. We sought to define the biochemical and physiological mechanisms that underlie biodegradative and other cellular processes in normal, extreme, and engineered environments. Toward that end, we sought to understand the substrate oxidation pathways, the electron transport mechanisms, and the modes of energy conservation employed during respiration by bacteria on soluble iron and insoluble sulfide minerals. In accordance with these general aims, the specific aims were two-fold:

(i) To identify, separate, and characterize the extracellular biomolecules necessary for aerobic respiration on iron under strongly acidic conditions; and

(ii) To elucidate the molecular principles whereby these bacteria recognize and adhere to their insoluble mineral substrates under harsh environmental conditions.

The results of these studies were described in a total of nineteen manuscripts. The highlights of these studies are briefly summarized below:

2. The complete genome of *Acidithiobacillus ferrooxidans* ATCC 23270 (type strain) was sequenced in collaboration with the DOE Joint Genome Institute.

This laboratory supplied the DNA to the US Department of Energy Joint Genome Institute for the determination of the DNA sequence of the entire genome of *At. ferrooxidans* ATCC 23270 (type strain). The genome consists of a single circular chromosome of 2,982,397 base pairs with a G+C content of 58.77%. A total of 3217 protein-coding genes were predicted, of which 2070 (64.3 %) were assigned a putative function.

On the basis of our analysis of the genomic data, the electron transfer pathway for the flow of electrons from iron to molecular oxygen in *At. ferrooxidans* is hypothesized to consist of an initial electron transfer from extracellular ferrous ions to a cytochrome *c* located in the outer membrane of this Gram-negative organism. The periplasmic blue copper protein, rusticyanin, then transfers the electron from the cytochrome *c* in the outer membrane to a different peri-plasmic cytochrome *c*. The final electron transfer is from the periplasmic cytochrome *c* to the terminal oxidase, an *aa3*-type cytochrome that is located in the cytoplasmic membrane and reduces molecular oxygen. This series of reactions is shown schematically in Fig. 1.

All three types of electron transport proteins were identified and readily visible in the preliminary ICAM (see item #8, below) long wavelength spectra shown in Fig. 2. All reduced *c*-type cytochromes possess a prominent absorbance peak at 551 ± 2 nm. Reduced cytochrome *c* is a principal feature in the iron-reduced spectrum of *At ferrooxidans* shown in Fig. 2. Similarly,

all reduced *a*-type cytochromes possess a prominent absorbance peak at 600 ± 10 nm. Reduced cytochrome *a* is also a principal feature in the iron-reduced spectrum shown in the figure. Finally, rusticyanin, a blue copper protein, has a broad absorbance band at around 600 nm in the oxidized state that disappears entirely when the protein is reduced. The presence of abundant

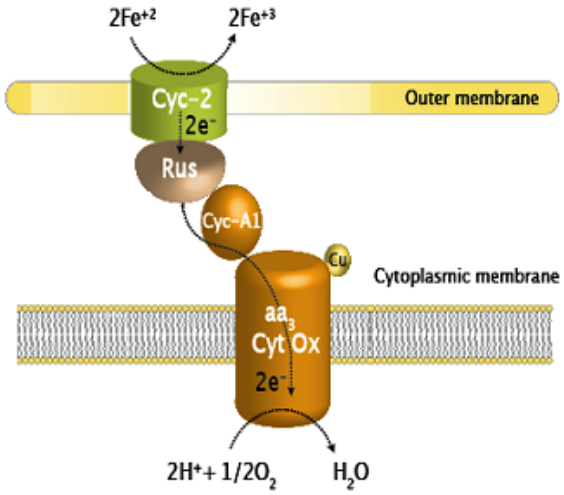

Figure 1. Schematic illustration of the electron transfer pathway hypothesized for aerobic respiration on ferrous ions by *At. ferrooxidans*

Figure 2. Preliminary ICAM spectra of oxidized (curve a) and iron-reduced (curve b) *At. ferrooxidans*

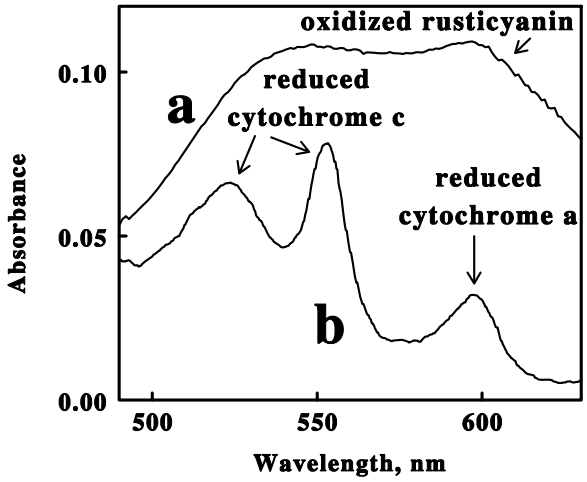

levels of rusticyanin is also evident in the two spectra shown in the figure. It is evident that the relevant electron transport proteins expressed by this particular autotrophic bacterium are all visible and may be studied relatively free from spectral interference by other colored molecules in the cell.

3. Genomic and mass spectrometry-based proteomic methods were used to evaluate gene expression and in situ microbial activity in a low-complexity natural acid mine drainage microbial biofilm community.

Gene expression, key activities, and the partitioning of metabolic functions were evaluated in a natural acid mine drainage microbial biofilm community. A total of 2,033 proteins were detected from the five most abundant species in the biofilm, including 48% of the predicted proteins from the dominant biofilm organism, *Leptospirillum* group II. Proteins involved in protein refolding and response to oxidative stress appeared to be highly expressed, which suggested that damage to biomolecules is a key challenge for survival. The relative abundance and cellular localization of 357 unique and 215 conserved novel proteins was estimated. Further, one abundant novel protein was shown to be a cytochrome (see item number 5, below) central to iron oxidation and acid mine drainage formation. To our knowledge, these studies represented the first effort to successfully analyze a natural community using these techniques.

4. Detailed functional and structural studies were conducted on rusticyanin, an acid-stable electron transfer protein purified from cell-free extracts of *At. ferrooxidans*.

The X-ray crystal structure of the oxidized form of the rusticyanin from *At. ferrooxidans* was determined by the method of multiwavelength anomalous diffraction (MAD) and refined to 1.9 Å resolution. Like other cupredoxins, rusticyanin was a copper-containing metalloprotein that was composed of a core β-sandwich fold. In rusticyanin the β-sandwich was composed of a six- and a seven-stranded β-sheet. Also like other cupredoxins, the copper ion was coordinated by a cluster of four conserved residues (His85, Cys138, His143, Met148) arranged in a distorted tetrahedron. Rusticyanin had a redox potential of 680 mV, roughly twice that of any other cupredoxin, and it was optimally active at pH values ≤2. By comparison with other cupredoxins, the three-dimensional structure of rusticyanin revealed several possible sources of the chemical differences, including more ordered secondary structure and more intersheet connectivity than other cupredoxins. The acid stability and redox potential of rusticyanin may also be enhanced over other cupredoxins by a more extensive internal hydrogen bonding network and by more extensive hydrophobic interactions surrounding the copper binding site. Finally, reduction in the number of charged residues surrounding the active site may also make a major contribution to acid stability. We proposed that the resulting rigid copper binding site, which was constrained by the surrounding hydrophobic environment, structurally and electronically favoured Cu(I). We also proposed that the two extreme chemical properties of rusticyanin were interrelated; the same unique structural features that enhance acid stability also led to elevated redox potential.

The solution structure of the Cu(I) form of the rusticyanin from *At. ferrooxidans* was also calculated from a total of 1979 distance and dihedral angle constraints derived from ^{1}H, ^{13}C and ^{15}N NMR spectra. The structures revealed two beta-sheets, one of six strands and one of seven strands that were tightly packed in a beta-barrel or beta-sandwich arrangement, and a short helix that extended on the outside of one of the sheets to form a second hydrophobic core. The copper coordination sphere was composed of the standard type I ligands (His2CysMet) in a distorted tetrahedral arrangement. The copper-binding site was located within a hydrophobic region at one end of the molecule, surrounded by a number of aromatic rings and hydrophobic residues. This configuration probably contributed to the acid stability of the copper site, since close association of the aromatic rings with the histidine ligands would sterically hinder their dissociation from the copper. An electrostatic analysis based on a comparison of the structures of rusticyanin and French bean plastocyanin showed that factors determining the high redox potential of rusticyanin include contributions from charged side-chains and from the disposition of backbone peptide dipoles, particularly in the 81 to 86 region of the sequence and the ligand cysteine residue. These interactions should also contribute to the acid stability by inhibiting protonation of His143.

5. An acid-stable red cytochrome with a novel absorbance peak at 579 nm was purified from cell-free extracts of *L. ferriphilum*.

A novel acid-stable red cytochrome that was expressed in abundant levels in *Leptospirillum ferriphilum* cultured on soluble ferrous ions was purified to electrophoretic homogeneity. This purified protein had an absorbance peak at 579 nm in its iron-reduced spectrum. The principal results obtained using the purified protein are summarized as follows:

(i) SDS-PAGE conducted on the purified cytochrome indicated a monomer molecular mass of around 16,000 daltons;

(ii) Visible absorbance spectra of cytochrome 579 were obtained for the oxidized native, reduced native, and oxidized and reduced alkaline pyridine hemochrome forms of the purified protein. These spectra are sufficient to demonstrate that cytochrome 579 possesses unique spectral characteristics that distinguish it from classic cytochromes *a*, *b*, *c*, *d* and *o*. Further studies on the chemical nature of this novel chromophore indicated that the heme group in cytochrome 579 was a derivative of heme *a* that was covalently attached to the apoprotein by a novel sulfhydryl bond;

(iii) The mass spectrum of the purified cytochrome 579 showed a major peak at 16,140 daltons;

(iv) Rayleigh light scattering experiments indicated that the soluble cytochrome 579 existed in an aggregated state of around 125,000 daltons, possibly consistent with an oligomer comprised of eight subunits;

(v) The amino terminal amino acid sequence of the purified cytochrome 579 was determined for the first 40+ residues; and

(vi) The oxidation and reduction kinetic behavior of the purified cytochrome 579 was determined by stopped flow spectrophotometric experiments conducted at pH 1.7 using ferric and ferrous ions, respectively. These observations established that cytochrome 579 was redox-active with soluble iron at acid pH.

The latter kinetic experiments were particularly interesting because atypical behavior was observed. When the concentration of soluble iron was varied, the rate of oxidation or reduction of the protein by ferric or ferrous ions, respectively, was not a linear function of the iron concentration, as was anticipated for a simple second order electron transfer reaction. Instead, the rate of reduction of the oxidized protein was proportional to the ferrous concentration raised to the power of 4.9, while the rate of oxidation of the reduced protein was proportional to the ferric concentration raised to the power of 3.9! One inevitable conclusion is that the redox potential of the purified cytochrome 579 changes with the concentration of soluble iron. That is, the standard reduction potential of the cytochrome is not a constant; rather, it increases as the iron concentration increases. This is a really unexpected and novel observation.

6. The specific adhesion of *At. ferrooxidans* to pyrite was mediated by an extracellular protein that was identified as aporusticyanin.

The binding of intact cells of *At. ferrooxidans* (ATCC 23270) to different sulfide minerals was investigated with three different techniques. First, the adhesion of intact cells to each mineral was quantified by counting the bacteria with electrical impedance measurements on a Multisizer IIe before and after incubation of the cells with the mineral. Secondly, the role of hydrophobic bonding in the adhesion event was studied by quantifying the surface hydrophobicities of minerals and cells cultured on different substrates using the FTA200 Dynamic Contact Angle system. Finally, the

force of adhesion of different bacteria to different minerals was quantified by optical trapping using a 200 mW set of LaserTweezers. When cultured on elemental sulfur as the sole source of energy, the adhesion of *At. ferrooxidans* to minerals was characterized by low affinity binding driven primarily by hydrophobic interactions that appeared to exhibit negligible specificity. When cultured on soluble ferrous ions as the sole source of energy, the adhesion of *At. ferrooxidans* to minerals was characterized by high affinity binding (an equilibrium dissociation constant of 5×10^{-15} M) that exhibited a high specificity for pyrite over other sulfide minerals; hydrophobic bonding appeared to play a minor role in the adhesion event. Indeed, the adhesion of iron-grown *At. ferrooxidans* to pyrite was so tight that we could only dissociate 7% of the bacteria adhered to the surface of the mineral using the LaserTweezers with the optical trap at full strength. In contrast, we could purposefully dissociate 94% of the cells previously cultured on sulfur under the same conditions.

The principal biopolymer involved in the adhesion of *At. ferrooxidans* to pyrite was identified and isolated by mineral affinity chromatography. Cell-free extracts of iron-grown *At. ferrooxidans* were introduced into a column packed with particles of pyrite. After exhaustive washing to remove cell debris, a solution of ferrous ions was passed through the column (ferrous ions serve to dissociate intact *At. ferrooxidans* from pyrite). A single colorless protein eluted in the ferrous ion wash. Amino acid sequence analysis from the N-terminus indicated that the sequence of the first 50 residues of this protein was identical to that of rusticyanin, an acid-stable blue copper protein in the electron transport chain of this organism. Further, the molecular mass of the protein eluted from the pyrite column was determined by mass spectrometry to be 16,549 daltons, only 3 daltons (or 0.02%) less than that determined by our laboratory in 1994 for aporusticyanin. Subsequent experiments demonstrated that wild-type aporusticyanin bound tightly to pyrite, while the holorusticyanin that contained one copper atom per polypeptide chain or the aporusticyanin in the presence of mM concentrations of ferrous ions did not.

The binding of recombinant aporusticyanin to different minerals was investigated. The adhesion of purified aporusticyanin to minerals was studied by quantifying the unbound protein that remained in solution after incubation with the mineral. Recombinant aporusticyanin was observed to adhere to different mineral with a pattern of reactivity identical to that observed with the intact bacterium. Further, preincubation of pyrite with excess exogenous aporusticyanin served to inhibit the adherence of intact cells to the surface of the mineral, indicating that the protein and the cells adhered to the pyrite in a mutually exclusive manner. Finally, preincubation of cells cultured on elemental sulfur (which do not express detectable aporusticyanin and do not bind specifically to pyrite) with recombinant aporusticyanin transformed the sulfur-grown cells into tight, specific pyrite-binding organisms. Substitution of alanine for His85, one of the 4 amino acid residues involved in copper ligation in the holorusticyanin, decreased the affinity of the aporusticyanin for pyrite by several orders of magnitude. This latter observation suggested that in the absence of copper, the same chelating residues are involved in the binding between the apoprotein and specific sites on the surface of the mineral.

Taken together, this body of work supports a model where aporusticyanin located on the surface of the bacterial cell acts as a mineral-specific receptor for the initial adherence of *At. ferrooxidans* to the solid. These experiments also serve as a model for analogous studies on the adhesion of other acidophilic iron-oxidizing organisms to mineral surfaces.

7. The specific adhesion of *L. ferriphilum* to pyrite was mediated by a different acid-stable extracellular protein than aporusticyanin.

Like *At. ferrooxidans*, *L. ferriphilum* adhered tightly to pyrite. The solid line and data points in Fig. 3 represent an isotherm for the binding of *L. ferriphilum* to pyrite in dilute sulfuric acid, pH 2.0. The free bacteria that remained in suspension after a two minute incubation with 0.1 g of pyrite were quantified by electrical impedance measurements. For comparison purposes, the dashed line in Fig. 3 represents the corresponding pyrite binding isotherm for *At. ferrooxidans* taken from the observations summarized above in item number 6. *L. ferriphilum* adhered to pyrite with an apparent equilibrium dissociation constant that was only about 5-fold higher (that is, 5-fold less affinity) than that of *At. ferrooxidans*. The fact that the maximum number of binding sites on pyrite was different for the two organisms suggested that they bind to different sites on the pyrite surface.

Cell-free extracts of *L. ferriphilum* were introduced into a column filled with crushed and sieved pyrite (average diameter of 75 μm) to capture and retain a putative pyrite binding protein that might be responsible for partially mediating the specific adhesion of the organism to pyrite. After washing the pyrite column until cellular components were no longer detected in the effluent (Fig 4, *lanes 2 and 3*), the column was washed with 100 mM ferrous sulfate, pH 2.0, to elute any cellular components that might be specifically adhered to the pyrite. A single colorless protein eluted in the ferrous ion wash; an SDS-PAGE analysis of the affinity-purified protein is shown in Fig. 4, *lane 4*. The apparent molecular mass of the pyrite binding protein in *L. ferriphilum* was 22,000 daltons. The actual mass of aporusticyanin is 16,549 daltons, although it migrates in SDS-PAGE with an apparent mass of 19,000 daltons. Further, *L. ferriphilum* is phylogenetically distinct from *At. ferrooxidans*, and neither holo- nor aporusticyanin could be detected in cell-free extracts of *L. ferriphilum*. These observations suggested that *L. ferriphilum* expresses a pyrite binding protein different from aporusticyanin.

A new method was developed to study the adhesion of selected chemolithotrophic bacteria to mineral surfaces in the presence of other bacteria with similar size, shape, and morphology. *At. ferrooxidans* was made highly fluorescent by exposure of the cells to SYTO 11™, a cell-permeant fluorescent nucleic acid intercalator that bound with high affinity and density to intracellular nucleic acids. The adhesion of fluorescently labeled *At. ferrooxidans* to pyrite was then studied using a KinExA 3000™ flow fluorimeter to concentrate and quantify the free, planktonic bacteria that failed to adhere to pyrite during passage of the suspended bacteria through a column of mineral particles. Prior adhesion of large numbers of unlabeled *At. ferrooxidans* to the pyrite strongly inhibited the subsequent adhesion of labeled *At. ferrooxidans* to the same sample of pyrite. Conversely, prior adhesion of large numbers of *L. ferriphilum* to the pyrite had very little effect on the subsequent adhesion of labeled *At. ferrooxidans* to the pyrite. Taken together, these observations suggest that these two organisms adhere to different sites on the surface of the pyrite using different biomolecules to achieve the observed high binding affinity. It is anticipated that this latter approach will permit investigators to study bacterial adhesion to minerals using mixtures of bacteria that more closely approximate those found in nature.

Figure 3

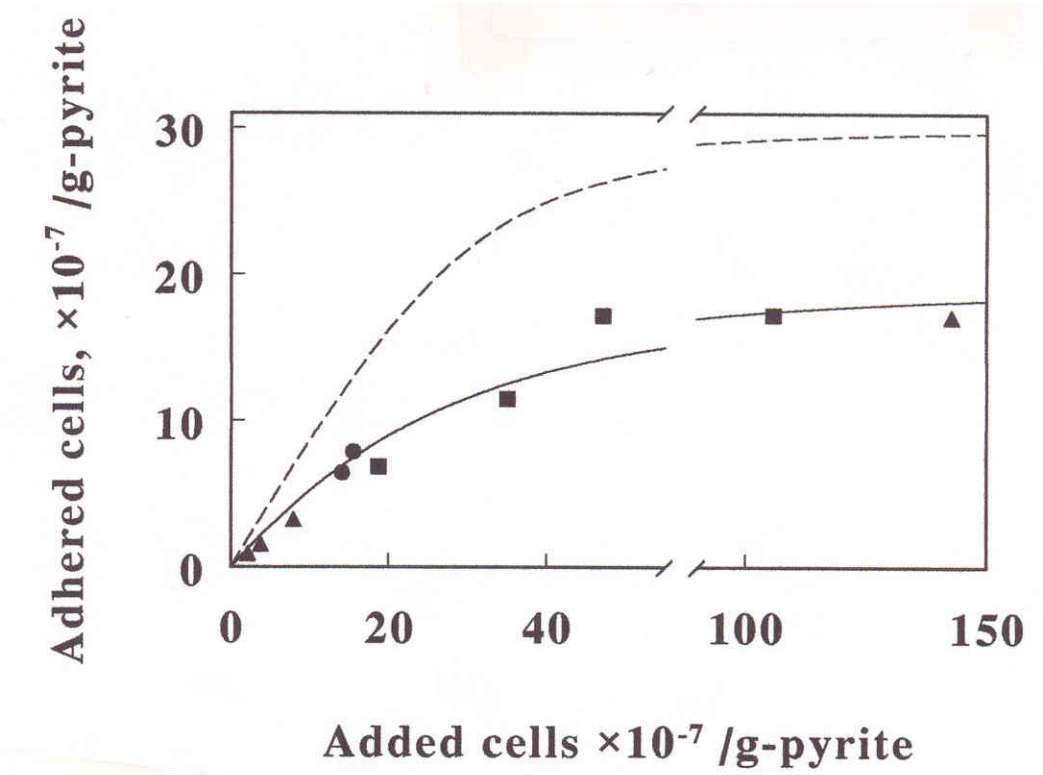

Figure 4

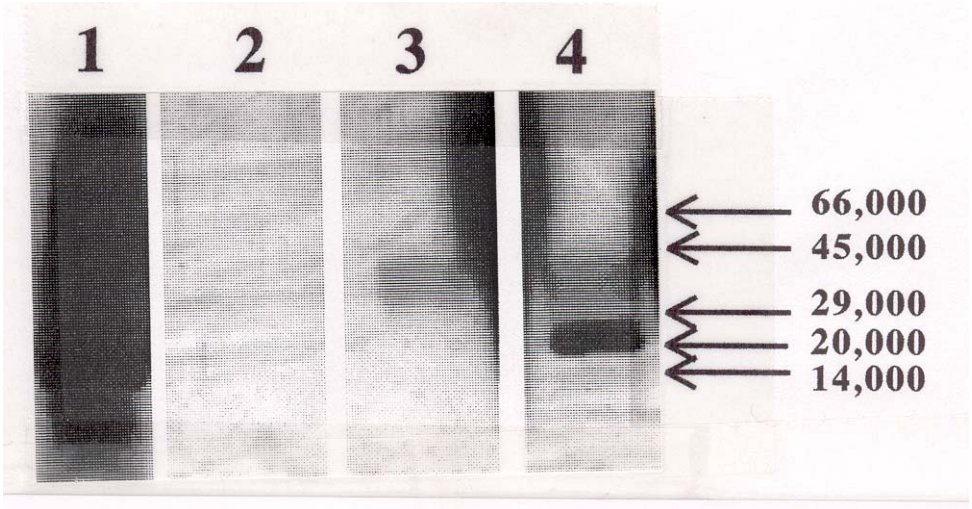

8. A prototype integrating cavity absorption meter (ICAM) was assembled to determine whether this novel spectrophotometer could be used to study cellular respiration *in situ*.

In collaboration with a commercial instrument company, a prototype integrating cavity absorption meter (ICAM) was assembled to determine whether this novel spectrophotometer would exhibit the two performance characteristics predicted for such an instrument : (i) that the ICAM would permit very sensitive absorbance measurements; and (ii) that the ICAM would permit accurate absorbance measurements even in highly turbid suspensions. Both expectations were realized: the 4.2 ml round quartz observation cell behaved as though it had an effective path length of >20 cm; and accurate spectra of purified cytochromes could be obtained even when they were dissolved in fat-free milk (data not shown). The principal features of this novel spectrophotometer used to conduct absorbance measurements in turbid solutions are included in the schematic diagram shown below in Fig. 5.

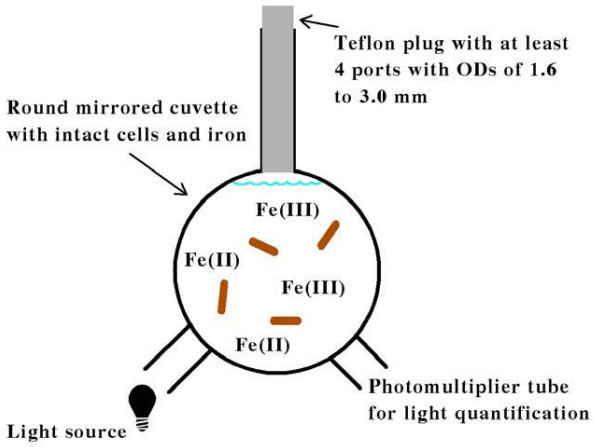

Figure 5. Schematic illustration of the ICAM constructed for this project

The sample and reference observation cells of this dual beam spectrophotometer were each comprised of a 4.2 ml spherical quartz cuvette fused with a 6 mm ID quartz tube. Each quartz chamber was surrounded by a tightly-packed white powder that served to maximize diffuse reflectance of light on the exterior walls of the spherical flask. The apertures in the reflecting sphere through which the measuring light entered and the transmitted/scattered light exited to the photomultiplier tube were positioned at a 90^{o} angle such that the light had to undergo many reflections and cell transversals before it was quantified using the photomultiplier tube. A white Teflon plug with a 6 mm OD was inserted into the quartz tube to minimize the loss of light out of the neck. A 1.0 cm white stir bar was included in the sample chamber to facilitate sample mixing and suspension of any particulate matter.

This new spectrophotometer was exploited to study the *in situ* aerobic iron respiratory chain of *Leptospirillum ferrooxidans* under physiological conditions. The aerobic respiratory chain of *L. ferrooxidans* was dominated by the redox status of the cytochrome 579. The cytochrome within the intact bacterium was reduced within the time that it took to mix a suspension of the bacteria with soluble ferrous iron at pH 1.7. Steady state turnover experiments were conducted where the initial concentrations of ferrous iron were less than or equal to that of the oxygen concentration. Under these conditions, the initial absorbance spectrum of the oxidized bacterium was always regenerated from that of the iron-reduced bacterium. The kinetics of aerobic respiration on soluble iron by intact *L. ferrooxidans* conformed to the

Michaelis-Menten formalism, where the reduced intracellular cytochrome 579 represented the Michaelis complex whose subsequent oxidation appeared to be the rate-limiting step in the overall aerobic respiratory process. The velocity of formation of ferric iron at any time point was directly proportional to the concentration of the reduced cytochrome 579. Further, the integral over time of the concentration of the reduced cytochrome was directly proportional to the total concentration of ferrous iron in each reaction mixture. These kinetic data obtained using whole cells were consistent with the hypothesis that reduced cytochrome 579 is an obligatory steady state intermediate in the iron respiratory chain of this bacterium.

The capability of conducting direct and accurate observation of absorbance changes *in situ* in intact organisms is a useful complement to traditional reductionist approaches and recent advances in proteomic and transcriptomic studies. The colored prosthetic groups of most electron transport proteins comprise intrinsic spectrophotometric probes whereby transient changes in the oxidation-reduction state of the proteins may be monitored with great sensitivity. There is no better means to establish physiological relevance in a metabolic function than to directly observe it as it occurs in the intact bacterium. The movement of electrons through electron transfer complexes is central to energy production in all living cells. The ability to conduct direct spectrophotometric studies under noninvasive physiological conditions represents a new and powerful approach to examine the extents and rates of biological events *in situ* without disrupting the complexity of the live cellular environment. Studies such as these should increase our fundamental understanding of biological energy transduction.